Journal of Geotechnical Geology

Journal homepage: geotech.iauzah.ac.ir

Zahedan Branch,
Islamic Azad University

Remote Sensing Performance in Locating the Economic Veins of Robat Karim Manganese Mine

Ebrahim Sharifi Teshnizi[1], Abdollah Yazdi*[2], Mohsen Golian[3]

[1]*Department of Geology, Faculty of Science, Ferdowsi University of Mashhad, Mashhad, Iran*
[2]*Department of Geology, Kahnooj Branch, Islamic Azad University, Kahnooj, Iran*
[3]*Department of Geology, Science and Research branch, Islamic Azad University, Tehran, Iran*

ARTICLE INFORMATION

Received 10 November 2021
Revised 11 December 2021
Accepted 20 December 2021

KEYWORDS
Robat Karim mine; Linemeants; Vein; Joint; Satellite image; Rose diagram.

ABSTRACT

Morphological analysis for extracting lineaments has widespread applications in tectonic and structural studies, hydrogeology, speleology, mineral exploration, and other related sciences. In this regard, aerial photographs, satellite images, and digital elevation models (DEMs) are widely used in these studies. One of the most common techniques for lineament extraction is preprocessing satellite images by applying filters such as edge detectors, color compositions, spectral classification, and spectral detection methods through related software and then lineament extraction through visual interpretation. In this paper, this technique was applied to extract the lineaments in the Robat Karim manganese mining area. Next, a Rose diagram was prepared to compare the trend of the lineaments along the host rock deposits and discontinuities. Overall, the results will be useful in determining the efficiency of extracting lines from satellite imagery in locating the mineral veins.

1. Introduction

Lineaments are map-able linear surface features distinguished from their neighboring feature patterns and are likely to represent subsurface phenomena (O'Leary et al., 1976, Hashim et al., 2013; Ahmadirouhani et al., 2017; Das and Pardeshi, 2017; Pour and Hashim, 2017; Das et al. 2018; Rajasekhar et al., 2018; Zhong et al., 2018). However, lineaments can be accepted as subsurface phenomena if the lines are created only by geological structures such as faults and fractures. Other lineaments in an area can be due to geomorphological phenomena (water channels and mountain ridges) and human activities (e.g., roads and farmland boundaries). Extracting and mapping the lineaments are among the most important issues in various fields such as suitable site selection for the dam, bridge, and road construction, in seismic and landslide hazard assessments (Stefouli et al., 1996), for mineral exploration and extraction (Rowan and Lathram, 1980), identifying hydrothermal sources, and hydrogeological research (Sabins, 1996). In hydrogeological and karst studies in rocky zones, areas prone to groundwater reservoirs and karst features are often found along fracture lines and faults. These geological features are often detected through lineaments on the earth's surface using satellite imagery in radar or visual spectra and digital elevation models (DEMs). In the exploration and survey of

* **Corresponding author.**
E-mail address: yazdi_mt@yahoo.com
Assistant Professor, Academic Staff.

https://doi.org/10.30495/geotech.2021.688783
Available online 24 December 2021
1735-8566/© 2021 Published by Islamic Azad University - Zahedan Branch. All rights reserved.

vein mineral deposits, since faults and fractures are a good place to concentrate minerals, the lineament extraction from satellite imagery can be a useful strategy in determining areas with mineralization potential.

Linemeant extraction can be done in two distinct ways, i.e., manually and automatically, through satellite imagery or a digital elevation model (DEM). After applying the appropriate filters, the lineaments are visually detected and extracted manually. On the other hand, in the automated method, the lineaments are simply extracted using methods such as the Hough Transform (Wang et al., 1990) or the LESSA computer program (Zlatopolsky, 1997).

2. Material and Methods

2.1. Geology of Robat Karim Mine

As shown in Fig. 1, Robat Karim Manganese Mine is located in the southwest of Tehran, 9 km northwest of Robat Karim city (50° 35′ to 51° 05′ E and 35° 26′ to 33° 35′ N. From the main Tehran-Saveh road, after passing through Robat Karim city, there is a road toward Parandak town and a military barracks. After driving 5 km on this road, there is a 4-km private road to the mine. Fig. 2 is provide the view of the mine. Robat Karim manganese mine is located in the central Iran zone and in the northeastern margin of the Urmia-Dokhtar volcanic belt. In this area, there is a significant expansion of lava and igneous rocks belonging to the Upper Eocene. The rocks are mostly pyroxene andesite, basaltic andesite, trachyte and rhyolite tuffs, and ignimbrite. In general, they have a relatively high potassium content such that their K2O/Na2O ratio is more than 1 in most cases. Manganese mineralization in this deposit is associated with trachyte and ignimbrite pyroclastic units (unit Ebr8) and gray to reddish-brown ignimbrite lavas (unit Eil9). In this region, minerals have formed and been concentrated in two phases. In the first phase, primary manganese mineralization has occurred in the trachyte and ignimbrite pyroclastic unit. This unit is identified by features such as stratigraphic position stability and evidence of formation in shallow marine to terrestrial environments. This unit has been introduced as a mineralized horizon and is outcropped only in the southeastern part of the mine. On this horizon, there are not many stratification traces, including romanechite, pyrolusite, cryptomelane, and brownite. The horizon appears as cement between breccia fragments or veins, small and large veins, and has a mass cauliflower texture scattered between the breccia fragments. Based on the available information, this deposit can be considered a syngenetic volcanic-sedimentary stratigraphic mineral horizon. The second part of the deposit consists of high-grade manganese veins characterized by structural constraints and limitations to specific stratigraphic units. In this part of the deposits, the minerals (i.e., romanechite, pyrolusite, and cryptomelane) have massive and cauliflower textures. Based on the available evidence, this part of the deposit, which is economically important, can be considered an epigenetic vein deposit. Chemical and geochemical evidence has shown that the fluids responsible for mineralization are supplied from the hydrothermal origin in each deposit section. This point is confirmed by the high Mn/Fe ratio, along with the positive correlation between manganese and O, Zn, As, Cu, and Sr elements.

Robat Karim mining area has developed following the Urmia-Dokhtar structural zone due to the effect of a right-handed shear system. The faults are mainly tensile in this system with a north-south strike. Based on geological studies conducted in Robat Karim mine (Alavi, 1990), the Robat Karim mine fault thrust in this area has played a critical role in distributing rock units and mineralization. The Robat Karim thrust has separated the red trachyte tufts and their upper units from the lower units. This fault has caused brecciation and folding of rocks in the hanging wall and footwall and the development of expansion-type cracks perpendicular to the fault's surface. The mine fault is a normal slope with an almost vertical slope, extending from the northwest to the southeast. The operation of this fault has ruptured the Robat Karim thrust (Arian, 1991). There are other faults in the mine that have locally displaced rock units. The movement direction of these faults is oblique and rotational, and they have an almost vertical slope along the northwest or northeast. Comparing the structural trend of the mining area and the direction of manganese veins shows that the thickest and most economical veins (8 to 0.5 m) correspond to the tensile faults of the region (type T). In contrast, the other veins that have a low thickness and no economic values are along the P and R type faults (among the main faults of the dextral shear system) (Fig. 4.).

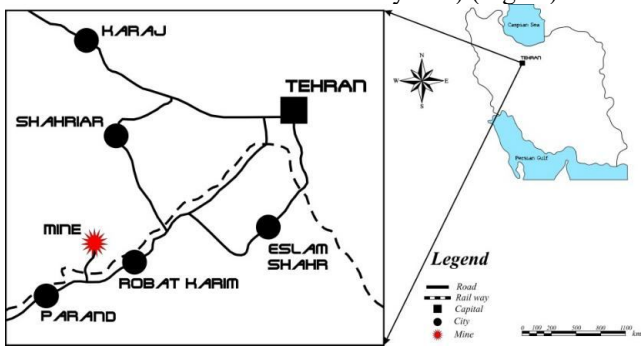

Figure 1. Location of Robat Karim manganese mine in Iran

Figure 2. A view of Robat Karim manganese mine

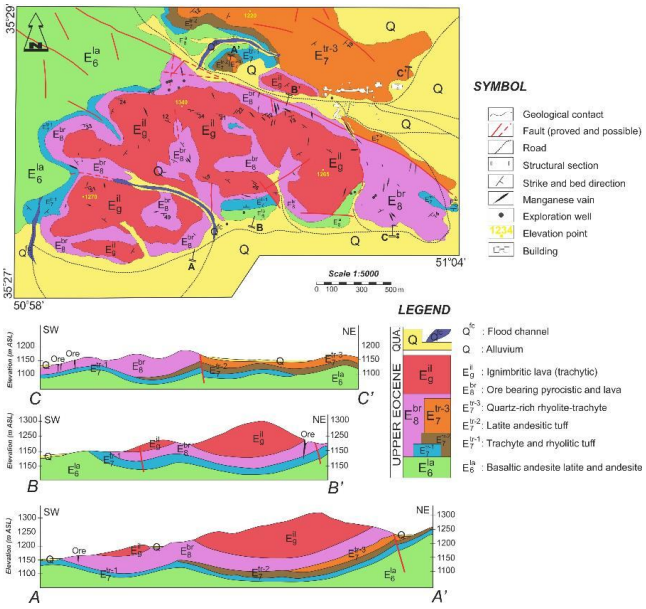

Figure 3. Geological map of Robat Karim mine (Amiri, 1995)

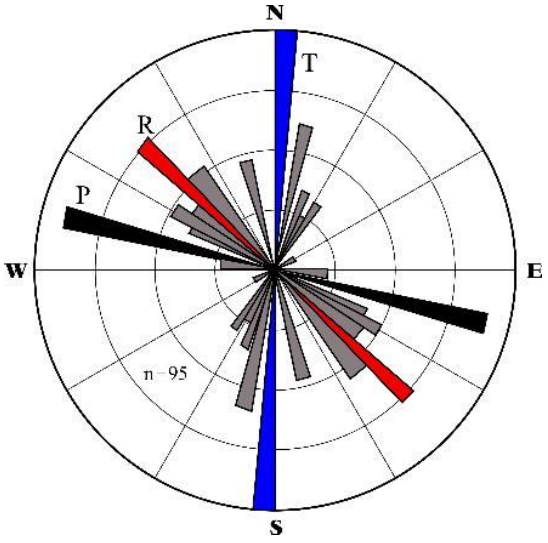

Figure 4. Rose diagram indicating the extension of manganese veins in the Robat Karim deposit (T: Veins corresponding to tensile faults, R: Veins corresponding to reverse faults, P: Veins corresponding to normal faults, Amiri, 1995)

2.2. Discontinuity Surveys

The joint condition and discontinuities of rock outcrops in the mining area due to the limited intact outcrops of the host rock mass were analyzed through some measurements performed in only four positions (Fig. 5).

In Station 1, trachyte and ignimbrite rocks (unit Ebr8) exposed by the ramp trench excavations were excavated (Fig. 6.). The rose diagram in Fig. 7 shows the joint survey results in this station. According to this diagram, in this unit, three joint sets (i.e., J1, J2, and J3) are detected with N30E, N40E, and N65E directions, respectively.

In Station 2, trachyte and igneous outcrops of unit Ebr8 were surveyed (Fig. 8). The results of this operation are represented as a Rose diagram in Fig. 9. According to this diagram, in the ignimbrite unit, three joint sets of J1, J2, and J3 with N07W, N15W, and N05E directions are detected, respectively. In Station 3, igneous lavas of the Eli9 unit were surveyed (Fig. 10). The rose diagram in Fig. 11 shows the geometry of all the seams of this outlet. According to this diagram, in this station, two joint sets of J1 and J2 with N05E and N65W directions are detected, respectively. In Station 4, outcrops of the igneous Eli9 unit with a stratified structure were surveyed (Fig .11). The rose diagram in Fig. 13 shows the results of this operation. As can be seen, there are three joint sets of J1, J2, and J3 with N20W, N40W, and N55W directions in this unit, respectively. Finally, combining all discontinuity information extracted from the mine surface (140 discontinuities), a rose diagram of the host rocks of manganese ore was drawn (Fig. 14). As can be seen, two main joint sets with dominant north-northeast and northwest directions, respectively, are distinguished in the rock masses of Robat Karim manganese mine.

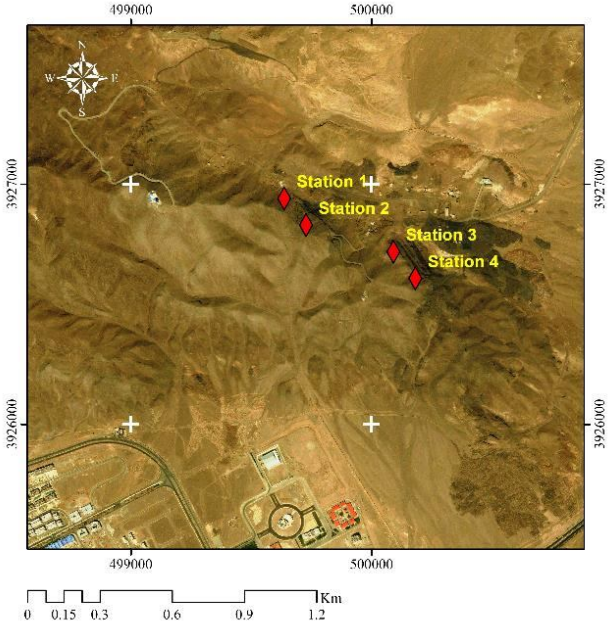

Figure 5. Discontinuities survey locations of Robat Karim manganese mine

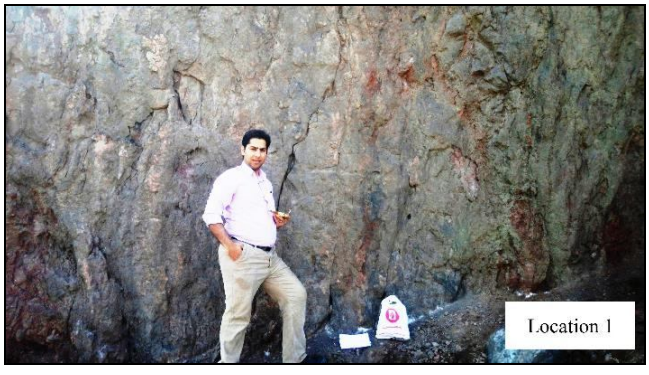

Figure 6. A view of the joint survey in Station 1

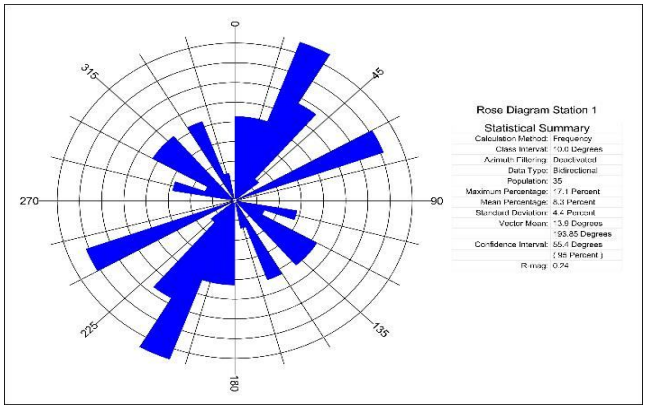

Figure 7. Rose diagram of joints for unit Ebr8 in Station 1

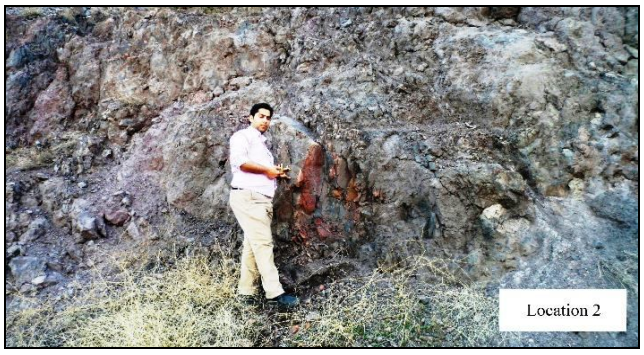

Figure 8. A view from Station 2

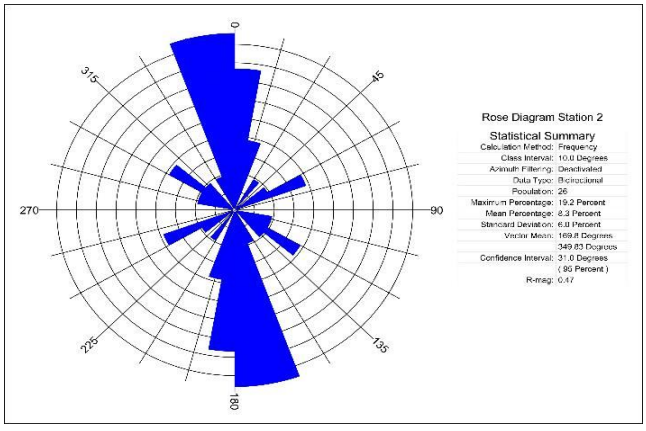

Figure 9. Rose diagram of unit Ebr8 joints at position 2

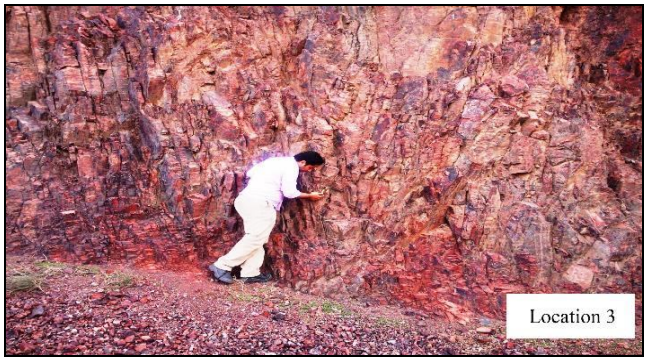

Figure 10. A view of the joint survey in Station 3

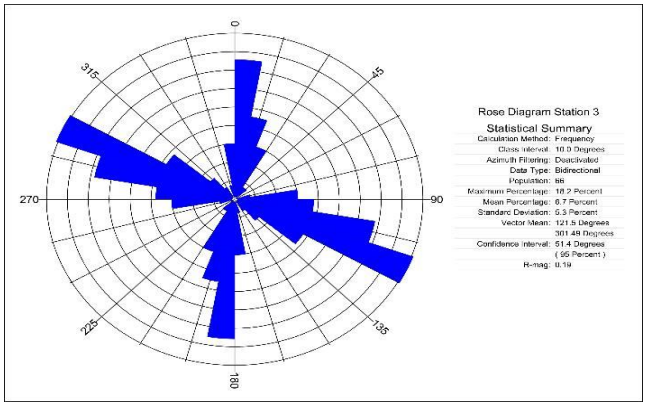

Figure 11. Rose diagram of joints for unit Eli9 in Station 3

Figure 12. A view of the joint survey in Station 4

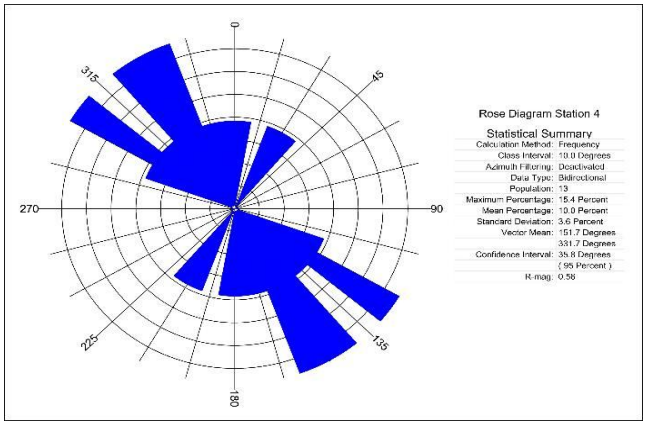

Figure 13. Rose diagram of joints for unit Eli9 in Station 4

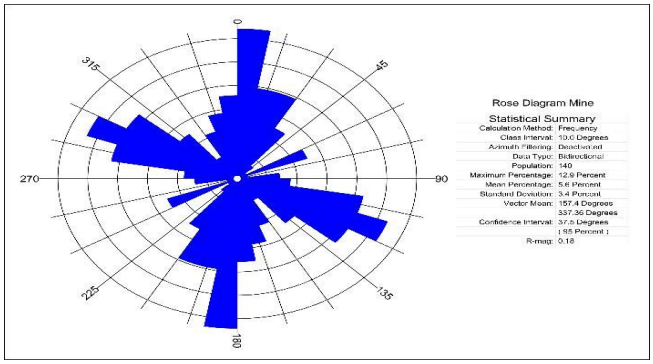

Figure 14. Rose diagram of ore host rocks at Robat Karim mine

3. Results and Discussions

3.1. Lineament extraction through satellite images

Manual lineament extraction operations include applying filtering operations, color compositing, spectral rationing, and principal component analysis (PCA) methods to satellite images and then lineament extraction through visual interpretation (Sarp, 2005). Filters are a part of the spatial enhancement operation, which is done based on the values of adjacent cells. Convolution, High-pass, Low-pass, and Edge detectors are among the major types of filters. The spatial detector is highly dependent on the spatial frequency. Spatial frequency is the degree of change in brightness at a unit distance in each part of an image. Loop filters are used to change the frequency profile of an image. High-pass filters allow high-frequency gray values to pass. These filters also facilitate edge (or linear features) detection in aerial photos. On the other hand, low-pass filters allow low-frequency gray values to pass through, blurring the image. The edge detection filter highlights the edges in the image, such as rivers, structural lines, and roads (Baba Ahmadi, 2009). PCA is a technique that produces images with an inter-correlation of 0 or almost 0. A major advantage of PCA is that the information in all image bands can be converted to a smaller number of bands without losing the band information (Baba Ahmadi, 2009). Since the human eye can only distinguish between a small numbers of gray color spectrums, with the color combination technique, the black and white satellite photos can be converted into a color image. Spectral segmentation of images is also usually performed to distinguish between spectral changes in an image covered by brightness changes.

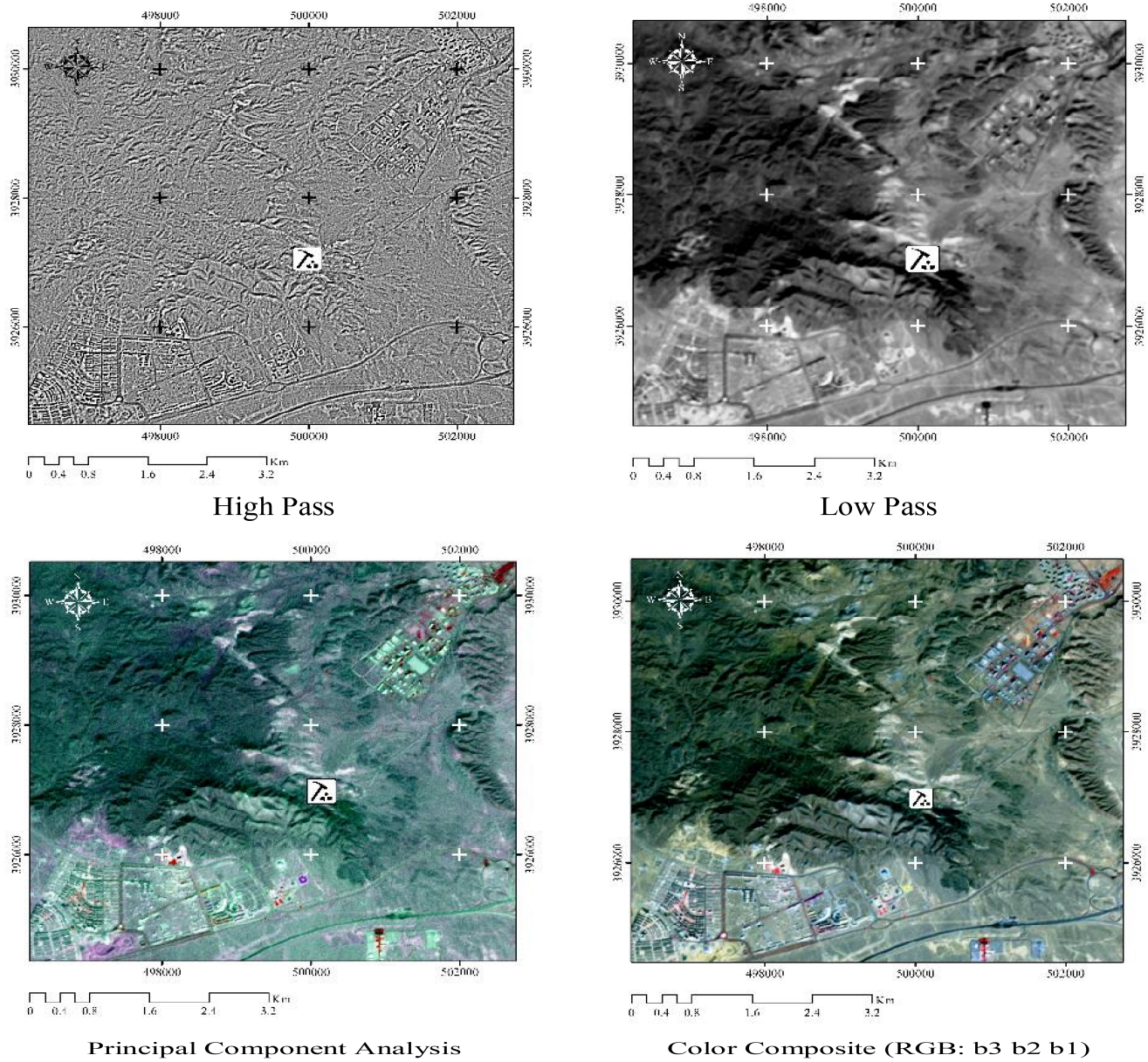

Figure 15. Highlighting the lineaments using the ETM image of the Landsat sensor

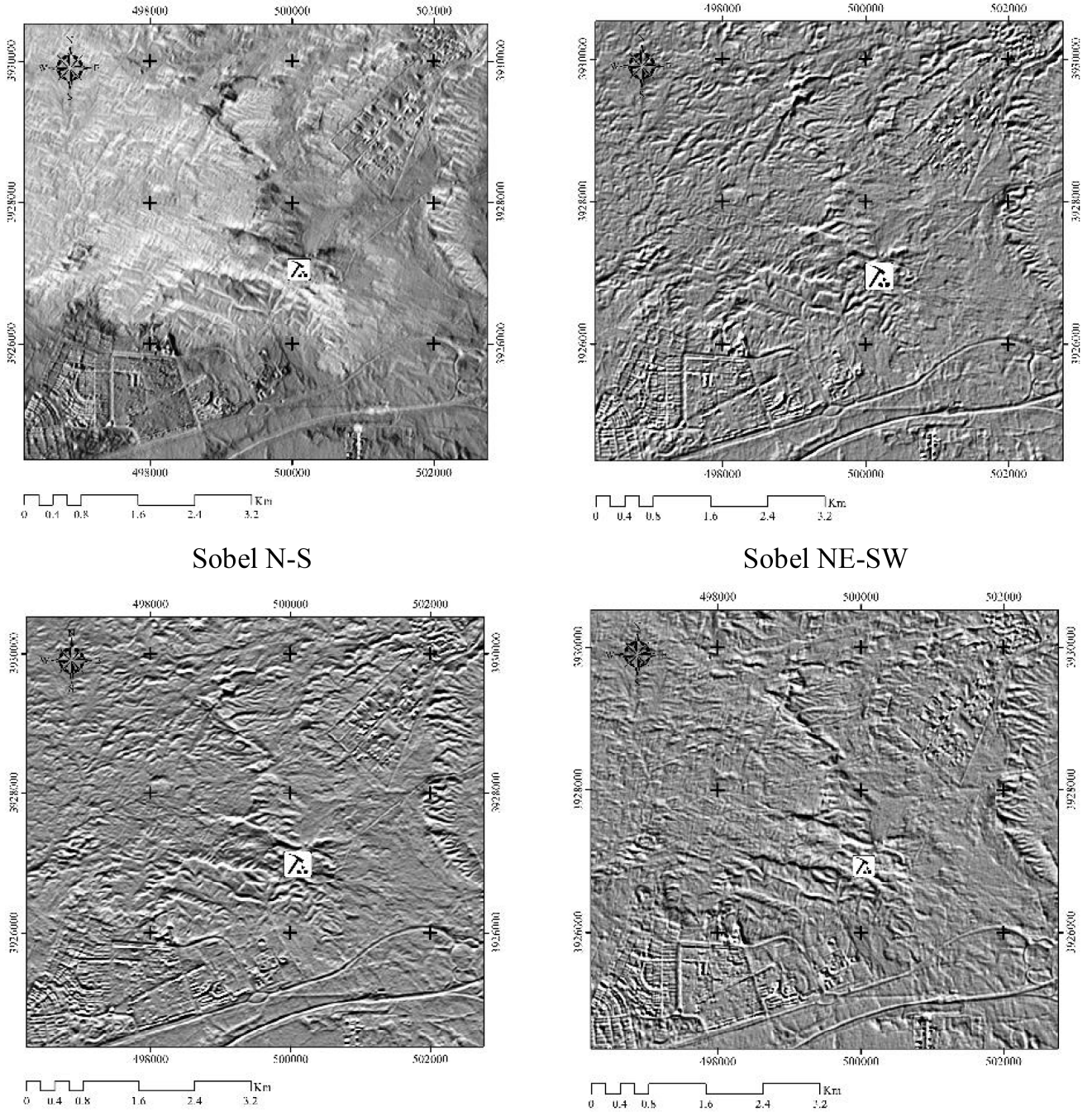

Figure 15. Continued

To make the lineaments more visible, we applied high-pass, low-pass, color composition (RGB: b3 b2 b1), PCA, and Sobel directional filters on ASTER Level 1 satellite image in Zone p164/r036, the results of which are shown in Fig. 15.

It is of note that directional filters are a type of edge detection filters that make spatial highlighting more prominent in one direction than in others. Thus, applying the filter in any direction makes the existing lineaments perpendicular to that direction more pronounced. Table 1 presents the Sobel filter operator matrix (with a 3 × 3-pixel kernel) used in this study in 4 main directions. Finally, to present the lines, the position of the lines in the map and the result of its statistical analysis are presented in a rose radiogram (Fig. 16). According to Fig. 16, the dominant direction of lineaments is in the northeast-southwest direction.

Table 1. Sobel filter operator matrix in four main directions

N-S			NE-SW			E-W			NW-SE		
-1	0	1	-2	-1	0	-1	-2	-1	1	1	2
-2	0	2	-1	0	1	0	0	0	-1	1	1
-1	0	1	0	1	2	1	2	1	-2	-1	0

3.2. The relationship between the lineaments and veins

As mentioned before, the dominant trend of the economic veins of the mine is north-northeast, while the dominant directions of the host rock masses are north-northeast and northwest (Fig. 17). As can be seen, deposit formation depends highly on tectonic structures, especially faults and fractures in the Robat Karim manganese mine. Also, these aspects allow extracting the lineaments accurately from the satellite image in detecting the economic veins from rock deposits.

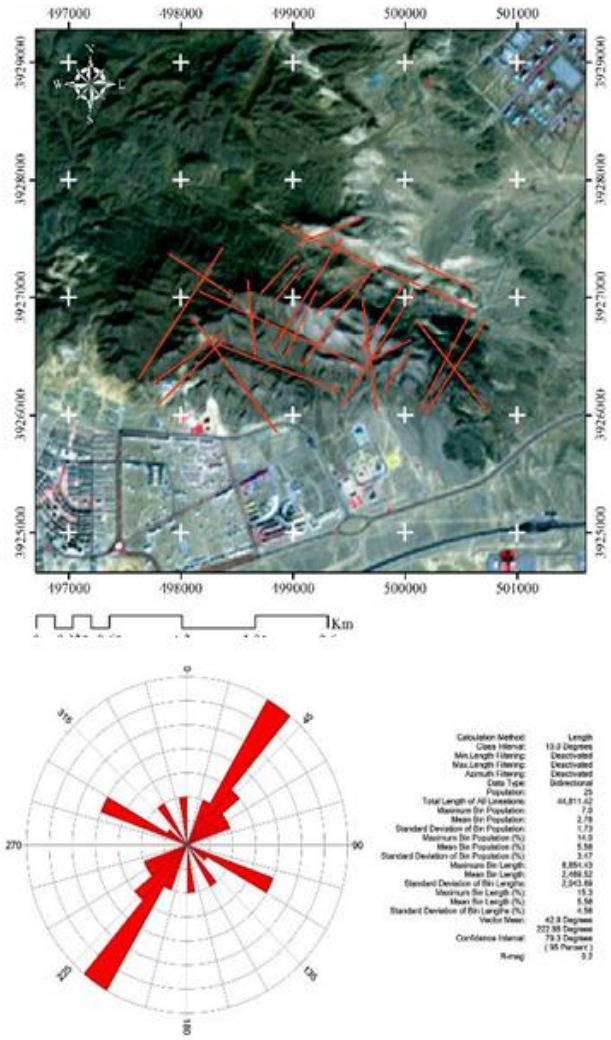

Figure 16. Location map and rose diagram of the lineaments identified in the area

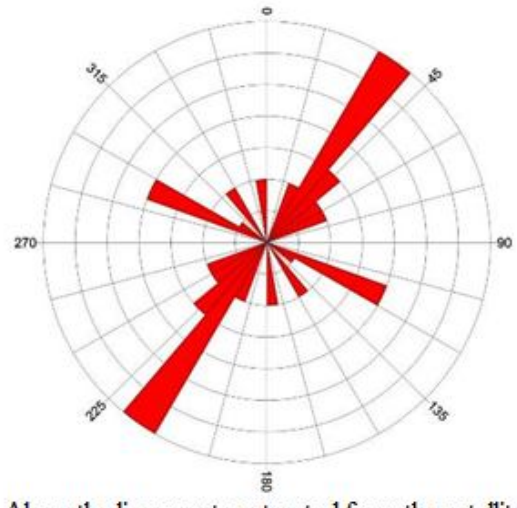

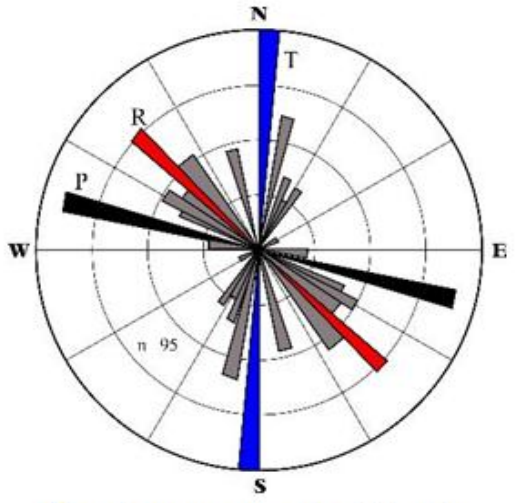

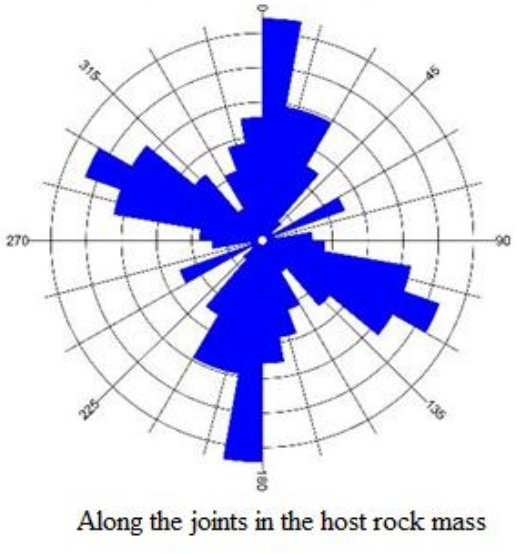

Figure 17. Comparing the directions of lineament extracted from the satellite photographs with the direction of the manganese veins of the mine and the discontinuities in its host rock units

4. Conclusion

Mineralization in many geological environments is highly controlled by faults and fractures. In the Robat Karim manganese deposit, this dependence also is remarkable in the Robat Karim manganese ore deposit such that in the mining area, manganese ore veins are abundantly seen in the late Eocene fractures and faults. This evidence indicates that the economic deposit of manganese ores is absolutely related to the region's tectonics. Therefore, in the present study, to confirm that the mineralization process follows structural controllers in the Robat Karim manganese mine, we extracted lineaments from the satellite image through a joint survey of host rock outcrops. Finally, the relationship between the orientations of these three cases was investigated by plotting the veins of the mine in a rose diagram. The results of these studies show a relatively high correlation between the lineaments extracted from the satellite image along the discontinuities and the manganese veins.

Acknowledgements

The authors wish to thank the Department of Geology, Ferdowsi University of Mashhad and Kahnooj Branch, Islamic Azad University for giving the permission of the study.

References

Abarca M.A.A., 2006. *Lineament extraction from digital terrain models (Case study: San Antonio del Sur area, South-Eastern Cuba)*. M.Sc. Thesis, International institute for geo-information science and earth observation enschede, Netherlands.

Ahmadirouhani R., Rahimi B., Karimpour M.H., Shafaroudi A.M., Najafi S.A., Pour A.B., 2017. Fracture mapping of lineaments and recognizing their tectonic significance using SPOT-5 satellite data: A case study from the Bajestan area, Lut Block, east of Iran. *Journal of African Earth Sciences*, 134: 600-612.

Alavi M., 1990. *Geological and tectonic study of Robat Karim mining area*. Ministry of Mines and Metals of the Geological Survey of Iran. [In Persian]

Amiri A., 1995. *Geological, mineralogical, and controlling factors of mineralization and concentration in Robat Karim manganese deposit*. M.Sc. Thesis, Tarbiat Modares University, Tehran. [In Persian]

Arian M.A., 1991. *Petrography and petrology of volcanic rocks in Robat Karim region*. M.Sc. Thesis, Tarbiat Moallem University, Tehran. [In Persian]

Baba Ahmadi A., 2009. *Applications of Remote Sensing (RS) in Geology*. Avaye Ghalam Publications, Tehran. [In Persian]

Das S., Pardeshi S.D., 2017. Comparative analysis of lineaments extracted from Cartosat, SRTM and ASTER DEM: a study based on four watersheds in Konkan region, India. *Spatial Information Research*, 26(1): 47-57.

Das S., Pardeshi S.D., Kulkarni P.P., Doke A., 2018. Extraction of lineaments from different azimuth angles using geospatial techniques: a case study of Pravara basin, Maharashtra, India. *Arabian Journal of Geosciences*, 11: 160.

Ganas A., Pavlides S., Karastathis V., 2005. DEM-based morphometry of range-front escarpments in Attica, central Greece, and its relation to fault slip rates. *Geomorphology*, 65: 301-319.

Hashim M., Ahmad S., Johari M.A.M., Pour A.B., 2013. Automatic lineament extraction in a heavily vegetated region using Landsat Enhanced Thematic Mapper (ETM^+) imagery. *Advances in Space Research*, 51(5): 874-890.

O'Leary D.W., Friedman J.D., Pohn H.A., 1976. Lineament, linear, lineation: Some proposed new standards for old terms. *Geological Society America Bulletin*, 87: 1463-1469.

Pour A.B., Hashim M., Makoundi C., Zaw K., 2016. Structural Mapping of the Bentong-Raub Suture Zone Using PALSAR Remote Sensing Data, Peninsular Malaysia: Implications for Sediment-hosted/Orogenic Gold Mineral Systems Exploration. *Resource Geology*, 66(4): 368-385.

Rajasekhar M., Raju G.S., Raju R.S., Ramachandra M., Kumar B.P., 2018. Data on comparative studies of lineaments extraction from ASTER DEM, SRTM and Cartosat for Jilledubanderu River basin, Anantapur district, A.P, India by using Remote Sensing and GIS. *Data in Brief*, 20: 1676-1682.

Rowan L.C., Lathram E.H., 1980. *Mineral exploration*. Chapter 17, in Remote Sensing in geology, John Wiley & sons, pp. 553-605.

Sabins F.F., 1996. *Remote Sensing: Principles and Interpretation (3rd Edition)*. W.H. Freeman and Company, 494 p.

Sarp G., 2005. *Lineament analysis from satellite images (North-West of Ankara)*. M.Sc. Thesis, Department of geodetic and geographic information technologies, Middle east technical university, Turkey.

Stefouli M., Angellopoulos A., Perantonis S., Vassilas N., Ambazis N., Charou E., 1996. Integrated analysis and use of remotely sensed data for the seismic risk assessment of the southwest Peloponessus Greece. In: *Proceedings of the First Congress of the Balkan Geophysical Society*, Athens.

Wang J., Howarth P.J., 1990. Use of the Hough transform in automated lineament detection. *IEEE Transactions on Geoscience and Remote Sensing*, 28: 561-566.

Wise S., 1998. *The effects of GIS interpolation errors on the use of digital elevation models in geomorphology*. In: Landform Monitoring, Modeling and Analysis, British Geomorphological Research Group Symposia, John Wiley & Sons Ltd., pp. 139-164.

Zhong Y., Ma A., Ong Y.S., Zhu Z., Zhang L., 2018. Computational intelligence in optical remote sensing image processing. *Applied Soft Computing*, 64: 75-93.

Zlatopolsky A.A., 1997. Description of texture orientation in Remote Sensing data using computer program LESSA. *Computers and Geosciences*, 23(1): 45-62.